Two-photon photoconductivity phenomena in semiconductors and insulators

Gad Koren
Microwave Division, The Racah Institute of Physics, The Hebrew University, Jerusalem, Israel
(Received 27 June 1974)

A comprehensive theoretical calculation of the spectral dependences of the two-photon photoconductivity (TPPC) measurements reported previously is given. The band-to-band two-photon absorption (TPA) was calculated by using an average-spherical-band model which was derived from the empirical pseudopotential band structure. The spectral dependences of the TPPC were calculated within the framework of the following three approximation schemes: (i) The $\vec{k}$ dependence of the transition-momentum matrix elements (MME) is ignored and real, constant, and equal MME are assumed for all the allowed transitions at $\vec{k} = 0$. (ii) The $\vec{k}$ dependences of the transition MME are calculated with the aid of the empirical pseudopotential wave functions, and the spherical averages of the absolute values of these MME are used in the calculations of the TPPC. (iii) The exact $\vec{k}$-dependent complex MME and energy bands are used, the summations over all the intermediate states are performed, and only the integration over $\vec{k}$ space is still carried out by using the average-spherical-band approximation. The results of these spectral TPPC calculations in a hexagonal ZnO crystal and in a mixed cubic and hexagonal ZnS crystal are given. For both crystals, and in all the approximation schemes, good agreement of the calculated TPPC with the experimental results was found, except for the energy region of the second transition in the ZnO crystal (4.25 eV), where only a partial agreement in the spectral shape of the TPPC with the measurements was found. Additional interesting theoretical results in the hexagonal crystals, obtained by a comparison with the experimental results, are that the pseudo-wave-functions of the deeper valence bands give only a poor representation of the real wave functions, and that occupied states should be taken into account as intermediate states in the two-photon transition probability. Alternative two-photon processes which may influence the TPPC, such as TPA by impurities, exciton TPA, and the reabsorption of second-harmonic-generated photons, are also considered, but mainly in a qualitative way.

I. INTRODUCTION

Since the development of the high-power lasers, two-photon spectroscopy investigation methods such as two-photon absorption (TPA), two-photon photoconductivity (TPPC), two-photon fluorescence, and second-harmonic generation have become very widely used. In these methods two photons instead of one participate simultaneously in the measured process. The importance of these investigative methods in comparison with the one-photon measurement method is that they enable us to achieve complementary information about the energy levels and band structures of materials as well as information about the nonlinear characteristics of the material. It is well known that optical transitions which are forbidden for one photon may be allowed for two photons. Therefore, using the two-photon methods, one can measure the forbidden one-photon energy gaps and the associated optical constants. Two additional important advantages of the two-photon measurement methods in solids in comparison with the known one-photon methods are: (i) For photons of energy $\hbar\omega$ such that $\hbar\omega < E_g$ but $2\hbar\omega > E_g$, where E_g is the energy gap of the material, two-photon processes (such as TPA and TPPC) take place in the bulk of the sample, whereas the equivalent one-photon processes involving photons of energy $2\hbar\omega$ will produce absorption on the sample's surface. This surface absorption makes the investigation of the bulk characteristics more difficult, if not impossible, because of the influence of surface recombination, surface states, surface imperfections, and so on. (ii) The possibility of using two different-frequency beams with different polarizations as the light sources provides us with a very powerful spectroscopic tool for the systematic investigation of materials, for example, identifying transitions according to the known selection rules. In this paper we will concentrate on TPPC phenomena and show the applications and the results of the general two-photon investigation methods for this case.

TPPC phenomena in solids have been investigated theoretically and experimentally by several authors.[1-14] These phenomena are due to the two-photon generation of free carriers in the illuminated sample and are closely related to the well-known two-photon absorption processes. Two-photon absorption spectroscopy has also been thoroughly investigated and often yields accurate results.[15-25] Until recently, most of the TPPC measurements in crystals were performed with a single monochromatic beam as the light source. The photoconductivity as a function of the intensity

of the beam is usually the sum of the one-photon and two-photon photoconductivities. In some cases, the measurements show a linear photoconductivity at low-light intensities and a parabolic rise at high intensities.[3,7] This then permits the separation of the TPPC from the one-photon photoconductivity. In many cases, however, the behavior of the photoconductivity as a function of the intensity I is not so simple. Nonlinear photoconductivities which are proportional to I^z, where z is not an integer, have been found experimentally.[6-9] (For example, using a Nd:glass laser $z = 1.8$ for GaAs and $z = 2.2$ for $CdS_{0.5}Se_{0.5}$ were measured.[8,9]) Yee[1] has shown from theoretical considerations, taking into account saturation and diffusion effects, that the TPPC behavior does not always have to be parabolic as a function of the beam's intensity; i.e., one cannot deduce in a simple way whether a given dependence of the photocurrent on intensity is caused by linear or nonlinear absorption effects. As a result of this difficulty, only a few spectral TPPC measurements were performed in the past. One such measurement was reported by Strome on anthracene[2] using one monochromatic beam at a few different discrete wavelengths. Recently, Bergman and Jortner have reported comprehensive photoconductivity measurements on anthracene using a tunable dye laser.[14] At each wavelength they measured the photocurrents as a function of the intensity of the source and this enabled the separation of the different contributions to the linear and nonlinear photoconductivity. This measurement procedure can yield the correct TPPC, but it requires an intensity-dependent measurement at each measured spectral point. Therefore, it is important to find simple measurement methods in which the pure TPPC part of the nonlinear photoconductivity measurement can be completely separated from the other linear and nonlinear contributions to the photoconductivity.

With these considerations in mind, we have developed a new measurement method which has enabled us to measure the net TPPC signals.[11-13] Two light sources of different frequencies are used. The sample is illuminated by both beams simultaneously and the photoconductivity signal is measured. In addition, the photocurrents from the crystal when illuminated with each source separately are also measured and subtracted from the result of the first measurement. The results obtained in this way are essentially free of one-photon and multiphoton effects which involve each beam separately. The use of this method enabled us to measure TPPC spectra quite accurately. Results for ZnS and ZnO crystals have already been reported.[12,13] In this paper an attempt will be made to explain these results qualitatively and quantitatively.

A calculation of the spectral and intensity dependences of TPPC with emphasis on the spectral behaviors will be presented here. The theory will be applied to the measurements previously made on ZnS and ZnO crystals. We will assume that there are two different-frequency radiation sources. The magnitude of the source photon energies and beam intensities will be assumed to be such as to yield "net TPPC,"[11] i.e., one source is weak and has a photon energy larger than half the crystal energy gap, the second source is strong and with photon energy smaller than half the crystal energy gap. The sum of the photon energy from both kinds of sources is larger than the crystal energy gap. We will also assume in the calculations that the light sources are randomly polarized and uniformly scattered on the crystals, as was the case in the experiments.[12,13]

In Sec. II the basic theoretical considerations concerning the TPPC phenomena in solids are presented. First, the two-photon generation rate of carriers in the crystal is given. In fact this generation rate is $W^{(2)}$, the known two-photon transition probability per unit volume and unit time. With the aid of $W^{(2)}$ one can determine, using the diffusion equation, the density of carriers in the crystal, which yields immediately the TPPC, as there is usually a simple linear dependence between them. It turns out that for fairly low intensities $W^{(2)}$ is linearly proportional to the product of the intensities of both beams in the crystal, where the proportionality constant depends on the photon energies and on the band structure of the crystal. These beam intensities were calculated previously as a function of the penetration depth in the crystal for one monochromatic beam[15] and for two monochromatic beams,[11] with the aid of the one-photon and two-photon absorption coefficient. However, because of some limiting assumptions concerning the beam intensities, made in Ref. 11, the calculation for two different monochromatic beams is repeated with less strict assumptions.

In Sec. III the results of the spectral dependences of the calculated TPPC for ZnS and ZnO crystals are presented. Three sets of calculations were performed. The first, and most simple, is a first-order approximation which assumes real, constant, and equal transition-momentum matrix elements for all the allowed transitions at $\vec{k} = 0$. The two forbidden transitions at $\vec{k} = 0$ included in this approximation are the transitions for which the highest valence and lowest conduction bands contribute as intermediate states in the second-order transition probability. Special expressions

for the intraband momentum matrix elements are derived for these transitions. The second approximation uses the $\vec{k}$-dependent momentum matrix elements. These are derived from the pseudopotential wave functions which were calculated separately. The third approximation involves the calculation of the momentum matrix elements and the band energies, which were derived from a complete pseudopotential band calculation. It also involves the summation over all the intermediate states which appears in the expression for $W^{(2)}$. For simplicity, averages of the effective masses and the momentum matrix elements were taken over the different $\vec{k}$ directions. The effective masses themselves were determined along the main symmetry axes from the $\vec{k}$ dependence of the energies. In this way an average-spherical-band model is obtained near $\vec{k}=0$, in a sphere whose radius is approximately one-third of the distance from Γ to A in the hexagonal Brillouin zone. The integrations over $\vec{k}$ space in all three approximations were performed analytically with the aid of the δ function which appears in the expression for the second-order transition probability $W^{(2)}$.

In Sec. IV the results obtained using the three calculation schemes of Sec. III are discussed and compared with the experimental results. In Sec. V the influence of other processes which yield TPPC is discussed qualitatively. The processes considered are the TPA by impurities, the reabsorption of the sum-frequency photons which are generated because of the nonlinear susceptibility of the crystal, and the TPA by exitons. Section VI contains the conclusions derived from the comparison of the theoretical and experimental results.

II. THEORY

The phenomenon of two-photon photoconductivity in solids involves the absorption of two photons in the crystal, which increases the crystal's conductivity. The two-photon generation of carriers in the crystals is mainly due to the two-photon absorption processes. In this section we shall discuss the band-to-band TPA, which yields the main contribution to the TPPC. The band-to-band TPA for two different light sources can be represented by $W^{(2)}$, the second-order transition probability per unit volume and unit time.[24] It is given by

$$W^{(2)}=\frac{1}{2\hbar}\left(\frac{e}{m}\right)^4\frac{\hbar N_1}{\epsilon_1\omega_1}\frac{\hbar N_2}{\epsilon_2\omega_2}\sum_{cv}\int d^3k\,|M_{cv}(\vec{k})|^2 \times\delta(E_c(\vec{k})-E_v(\vec{k})-\hbar(\omega_1+\omega_2)), \quad (1)$$

where N_1 and N_2 are the photon densities of the beams with frequencies ω_1 and ω_2, respectively, ϵ_1 and ϵ_2 are the corresponding dielectric constants, and the summation over c and v is a summation over the contributing valence and conduction bands. $E_i(\vec{k})$ is the energy of the ith band at $\vec{k}$ and the composite matrix element $M_{cv}(\vec{k})$ is given by

$$M_{cv}(\vec{k})=\sum_j\left(\frac{(\vec{e}_1\cdot\vec{P}_{cj}(\vec{k}))(\vec{P}_{jv}(\vec{k})\cdot\vec{e}_2)}{E_j(\vec{k})-E_v(\vec{k})-\hbar\omega_1}+\frac{(\vec{e}_2\cdot\vec{P}_{cj}(\vec{k}))(\vec{P}_{jv}(\vec{k})\cdot\vec{e}_1)}{E_j(\vec{k})-E_v(\vec{k})-\hbar\omega_2}\right), \quad (2)$$

where $\vec{e}_1$ and $\vec{e}_2$ are unit vectors in the direction of polarization of the corresponding beams and $\vec{P}_{ij}(\vec{k})$ are momentum matrix elements between the ith and the jth bands. [The factor $\frac{1}{2}$ which appears in Eq. (1) is missing from Eq. (2) of Ref. 24. This is probably a result of different assumptions made here as opposed to those of Ref. 24.] In this paper the form of the radiation electric field is assumed to be $\vec{E}_0\cos\omega t$ and the summation over the c and v bands includes spin and degeneracies. $W^{(2)}$ may be written in the following short form:

$$W^{(2)}=AI_1I_2, \quad (3)$$

where A is a constant which depends on the band structure of the crystal and the two photon energies, and I_1 and I_2 are the intensities of the beams whose frequencies are ω_1 and ω_2, respectively. The relation between I_i and the photon density N_i for $i=1, 2$ is given by

$$I_i=(c/\sqrt{\epsilon_i})\hbar\omega_i N_i. \quad (4)$$

The TPPC $\sigma^{(2)}$ is defined by the equation

$$\vec{J}=\sigma^{(2)}\vec{E}=N^{(2)}e\mu\vec{E}, \quad (5)$$

where $\vec{J}$ is the photocurrent density, $\vec{E}$ is the external electric field, $N^{(2)}$ is the two-photon-generated charge density, e is the electron charge, and μ is the mobility. If the carrier lifetime τ satisfies $\tau\ll T_r$ where T_r is the duration of the radiation pulse, and if diffusion effects are neglected, then the carrier concentration satisfies the following simple equation

$$N^{(2)}=W^{(2)}\tau. \quad (6)$$

Equations (5) and (6) may be recombined now to yield the desired TPPC

$$\sigma^{(2)}=W^{(2)}e\mu\tau. \quad (7)$$

Equation (7) shows immediately that in order to compare the experimental $\sigma^{(2)}$ with theory it is not sufficient to calculate $W^{(2)}$, but one also has to know μ and τ. For convenience, the TPPC notation $\sigma^{(2)}$ will not be used in the continuation of this paper, and the short notations σ for the experimentally measured TPPC and σ' for the cal-

culated TPPC will be used instead.

Let us now examine the behavior of the TPPC as a function of the beam intensities and assume that the wavelengths of the two sources are constants. Let us also assume that the intensities and wavelengths of the beams were chosen in such a way that the TPA is always due to two photons, one from each beam.[11] If the beams penetrate perpendicularly to a depth x in the crystal, then their intensities due to one-photon and two-photon absorption behave according to the following equations[11]:

$$dI_1/dx = -\alpha_1 I_1 - \beta I_1 I_2 , \tag{8}$$

$$dI_2/dx = -\alpha_2 I_2 - \beta I_1 I_2 , \tag{9}$$

where α_1 and α_2 are the linear absorption coefficients of the beams at frequencies ω_1 and ω_2 respectively, and β is the two-photon absorption coefficient. Nontrivial analytic solutions for the exact conjugate Eqs. (8) and (9) are not available, but approximate solutions are easily obtained instead. One such solution was given in Ref. 11. It was assumed there that I_1, the weak beam, may be chosen weak enough to satisfy the inequality $\beta I_1 \ll \alpha_2$; i.e., the absorption of the strong beam I_2 is mainly due to linear absorption. In this case,

$$I_2(x) = I_{20} e^{-\alpha_2 x} , \tag{10}$$

and substituting this I_2 in Eq. (8) yields

$$I_1(x) = I_{10} \exp[-\alpha_1 x - (\beta I_{20}/\alpha_2)(1-e^{-\alpha_2 x})] . \tag{11}$$

One can see that, at a given penetration depth x, the absorption of the I_1 beam is increased exponentially by increasing the intensity of the I_2 beam. However, the assumption that the weak beam I_1 satisfies $\beta I_1 \ll \alpha_2$ does not always hold. Therefore, in order to reduce this limitation on the beam intensities, Eqs. (8) and (9) will be solved within a different approximation. In this approximation one assumes that the linear absorption coefficient of the one beam is approximately equal to that of the other, i.e., $\alpha_1 \approx \alpha_2$. This approximation seems reasonable, since these linear absorptions are due to the defects and impurities in the band gap of the crystal. Usually, impurities have fairly narrow bands in the band gap of the crystals. However, for different kinds of impurities a certain spread of the impurity energy levels occurs, and for photons of similar energy ($\omega_1 \approx \omega_2$) the approximation $\alpha_1 \approx \alpha_2$ is quite a good one. Using this approximation and substituting

$$I_i(x) = J_i(x) e^{-\alpha_i x} \tag{12}$$

for $i = 1, 2$ in Eqs. (8) and (9) one obtains

$$J_2(x) = J_1(x) + c , \tag{13}$$

where c is the constant $I_{20} - I_{10} = I_2(0) - I_1(0)$. Equation (8) is solved now with the aid of Eqs. (12) and (13). This yields

$$I_1(x) = I_{10}[(I_{20} - I_{10}) e^{-\alpha_1 x}] \times (I_{20} \exp\{[\beta(I_{20} - I_{10})/\alpha_2](1 - e^{-\alpha_2 x})\} - I_{10})^{-1} . \tag{14}$$

$I_2(x)$ is easily obtained with the aid of Eqs. (12) and (13). It is clear in Eq. (14) that although we assumed $\alpha_1 \approx \alpha_2$, we still separate between α_1 and α_2. This seems to be a better approximation to the real expression for $I_1(x)$, since the relation $\alpha_1 = \alpha_2$ was used only at the stage of obtaining Eq. (13). Equation (14) is more general than Eq. (11) (which was also used in Ref. 11). Equation (14) is reduced to Eq. (11) if one assumes that $I_{20} \gg I_{10}$ and notes that $\beta(I_{20} - I_{10})/\alpha_2 > 0$ and $e^{-\alpha_2 x} \leq 1$. Hence Eq. (11) is a good approximation even without the assumption that $\beta I_1 \ll \alpha_2$ and it is enough to assume $\alpha_1 \approx \alpha_2$ and $I_2 \gg I_1$ in order to satisfy this equation.

The concentration P of the two-photon carriers in the crystal is determined with the aid of the diffusion equation[11]

$$-D \frac{\partial^2 P(x,t)}{\partial x^2} + \frac{\partial P(x,t)}{\partial t} = W^{(2)} - \frac{P(x,t)}{\tau} , \tag{15}$$

where D is the diffusion constant and τ is the bulk lifetime of the carriers.

$W^{(2)}$ is defined in Eq. (3) [the short form of Eq. (1)] and the I_1 and I_2 are given in Eqs. (14) [or Eq. (11)] and (13). J. Yee[1] has solved the diffusion equation [Eq. (15)] assuming (i) a steady-state condition (i.e., $\partial P/\partial t = 0$), (ii) that $\omega_1 = \omega_2$, and (iii) using the generation rate obtained by Basov *et al.*[16] In his calculations Yee neglected the linear absorption of the beam. However, Eq. (11) here can be reduced to the form of the beam intensity used by Yee simply by assuming that $\alpha_2 x \ll 1$ and that $\alpha_1 x \ll \beta I_{20} x \ll 1$. Hence, with these limitations Yee's results are valid in our case as well. It is possible, of course, to repeat Yee's calculations with the more exact expression of the generation rate of Eq. (14). In this way one obtains the theoretical predictions for the intensity-dependent TPPC found in our previous results.[11,12] But since no significant change in Yee's results was expected for our case, no new calculation concerning the intensity-dependent TPPC was performed.

The intensity-dependent photoconductivity measurements with one monochromatic beam show that in some experiments the TPPC is exactly parabolic as a function of the beam intensity I,[2,3,4,7] while in other measurements the TPPC is proportional to I^z where $z \neq 2$.[6-9] The actual value of z depends on the intensity of the incident laser beam,

the thickness of the sample and the different recombination processes involved. The saturated TPPC behaviors, for which $z<2$, can still be understood within the framework of the existing theories.[1] An inspection of the expressions for the beam's intensity as a function of its penetration depth [see Eqs. (11) or (14) here, and Eq. (11) in Ref. 16] reveals that the increase in the beam's intensity yields a higher absorption near the crystal surface. This absorption yields a heavier carrier concentration close to the sample's surface, which saturates the TPPC because of the higher recombination rate on the surface. However, Yee's results[1] for two-photon excitation processes are not applicable in cases where $z>2$. To explain the TPPC behavior in these cases one has, for example, to allow for an intensity-dependent carrier lifetime. Such an intensity-dependent lifetime effect was observed in the intensity-dependent TPPC measurement in ZnS, where a ruby laser and a Rodamine dye laser were used as the light sources.[11,12] In this measurement the intensity of the dye laser beam was held constant and the TPPC, as a function of the intensity of the ruby laser beam, shows two consecutive linear behaviors with a greater slope of the TPPC in the region of the high intensities. This clearly indicates a saturation of one recombination channel which yields the measured increase in the TPPC.

To summarize, the results of the intensity-dependent behaviors of TPPC for fairly low laser intensities, and for not too thin crystals are (i) no saturation effects due to heavier surface recombination occur, (ii) TPPC is proportional to I^2 if we use one monochromatic beam, or to $I_1 I_2$ if two different-frequency beams are used.

Let us now examine the spectral dependencies of TPPC. The coefficient A in Eq. (3), or the coefficient of $N_1 N_2$ in Eq. (1), contains the influence of the band structure on the TPPC via $W^{(2)}$. In order to examine this influence carefully, it is desirable to calculate it step by step and to try to separate its different contributions. We will begin with a first-order approximation in which it will be assumed that the energy bands are spherical and that all the allowed transition momentum matrix elements (MME) are real, constant, and equal. Since both photon energies, $\hbar\omega_1$ and $\hbar\omega_2$, are taken to be less than the band gap of the crystal, no linear band-to-band absorption is possible. We therefore may also assume that the energy denominators in Eq. (2) do not change rapidly as a function of the photon energy. These assumptions immediately yield the result that $W^{(2)}$ behaves like the joint density of states of the c and v bands.[26] This crude approximation usually yields the right prominent structures of the TPPC spectra but often fails to give the fine structures. There are two main sources for this failure in our case. One is the $\vec{k}$ dependence of the MME and the other is the nonparabolic $\vec{k}$ dependence of the energy bands. The first problem may be solved partially in a very simple way which is still within the framework of the constant MME approximation scheme, and which will be described. The second problem is more complicated and will be referred to at the end of this section.

Let us first examine the specific terms in Eq. (2), which describe the transitions from the v bands to the c band for which the intermediate states j are the v and c bands themselves. Two types of MME involved with these transitions are P_{vv} and P_{cc}. In the Appendix the analytical expressions for these MME (for nondegenerate v and c bands) are derived. [See Eq. (A8) of the Appendix.] The conditions in which Eq. (A8) is valid for degenerate bands are also discussed in the Appendix. Substituting (A8) in Eq. (2) yields

$$M_{cv}(\vec{k})=\sum_{\substack{j\\ j\neq c,v}}\left(\frac{(\vec{e}_1\cdot\vec{P}_{cj}(\vec{k}))(\vec{P}_{jv}(\vec{k})\cdot\vec{e}_2)}{E_j(\vec{k})-E_v(\vec{k})-\hbar\omega_1}+\frac{(\vec{e}_2\cdot\vec{P}_{cj}(\vec{k}))(\vec{P}_{jv}(\vec{k})\cdot\vec{e}_1)}{E_j(\vec{k})-E_v(\vec{k})-\hbar\omega_2}\right)+\hbar\left(\frac{m}{m_c^*}-\frac{m}{m_v^*}\right)\times\left(\frac{(\vec{e}_1\cdot\vec{k})(\vec{P}_{cv}(\vec{k})\cdot\vec{e}_2)}{\hbar\omega_2}+\frac{(\vec{e}_2\cdot\vec{k})(\vec{P}_{cv}(\vec{k})\cdot\vec{e}_1)}{\hbar\omega_1}\right). \tag{16}$$

Using the approximation of spherical bands, real, constant and equal MME and slowly varying energy denominators in Eq. (16), two limiting cases are easily obtained in the energy region near the crystal gap: when the first term in Eq. (16) is dominant,

$$W^{(2)}\approx\int k^2\,dk\,\delta\left[\frac{\hbar^2k^2}{2}\left(\frac{1}{m_c^*}-\frac{1}{m_v^*}\right)-[\hbar(\omega_1+\omega_2)-E_g]\right], \tag{17}$$

and when the second term in Eq. (16) is dominant,

$$W^{(2)}\approx\int k^4\,dk\,\delta\left[\frac{\hbar^2k^2}{2}\left(\frac{1}{m_c^*}-\frac{1}{m_v^*}\right)-[\hbar(\omega_1+\omega_2)-E_g]\right]. \tag{18}$$

Equations (17) and (18) are immediately integrated and yield

$$W_a^{(2)}\approx[\hbar(\omega_1+\omega_2)-E_g]^{1/2}, \tag{19}$$

$$W_b^{(2)}\approx[\hbar(\omega_1+\omega_2)-E_g]^{3/2}. \tag{20}$$

Usually a mixed behavior of $W_a^{(2)}$ and $W_b^{(2)}$ occurs, and as will be seen later on, it will be possible to fit even this crude model to our experimental results in the ZnS and ZnO crystals.

Next we consider a somewhat more realistic band model. We will still assume spherical bands but the $\vec{k}$ dependence of the MME in $W^{(2)}$ will be taken into account. We calculate the MME using the empirical-pseudopotential band calculation scheme.[26-29] The results of this calculation will be presented and discussed in Sec. III. Here we will only note that $\vec{P}_{ij}(\vec{k})$, (i.e., the MME as a function of $\vec{k}$) are certainly not real and not constants. In a separate calculation the composite matrix elements of Eq. (2) are computed exactly from the pseudopotential calculation. The MME and the energy bands are computed as a function of the wave vector $\vec{k}$ and the sums over all the contributing intermediate bands are performed.

In all the approximations an average spherical band model is used. An average of the MME and of the composite matrix elements in Eq. (2) is also taken over the different $\vec{k}$ directions. The validity of these approximations will be discussed in the next section. Here it will merely be noted that these last mentioned averagings allow us to carry out the integration in Eq. (1) over $\vec{k}$ space with the aid of the δ function, which saves us a lot of trouble in carrying out the numerical integration over $\vec{k}$ space. Therefore, the TPPC results which are obtained analytically are much more rigorous.

Finally, the influence of the nonparabolic and nonanalytic bands on the spectral dependences of the TPPC will be considered briefly. The $\vec{k}$ dependence of the energy bands affects the TPPC mainly through the joint density of states of the valence and conduction bands which are under consideration, i.e., the more important influence of the shape of the bands on the TPPC spectra is due not to the energy denominators which appear in Eq. (2) (unless there is a resonant term there), but to the δ function which appears in the integrand of Eq. (1). Hence, even a linear $\vec{k}$-dependent valence band, for example, does not greatly change the results of Eqs. (19) and (20). This is because the lowest conduction band remains parabolic. Therefore, the energy difference between the conduction band and the valence bands is also parabolic in $\vec{k}$. The more severe problem of the influence of the nonanalytic bands on the shape of the joint density of states, especially at regions of nonanalytic critical points, was treated thoroughly by Phillips.[30] The results of Phillips's work are immediately applicable to our problem of the influence of the nonanalytic bands on the shape of the TPPC spectra.[13]

III. RESULTS

The band parameters used in calculating the TPPC were obtained with the aid of the empirical-pseudopotential method[28] (EPM). Bergstresser and Cohen[27] had previously reported EPM calculations for hexagonal and cubic ZnS crystals. More recently, Bloom and Ortenburger[29] carried out similar calculations for hexagonal ZnO crystals. These calculations have been repeated here using the same form factors. For the hexagonal structure, 67 plane waves form the basis for the representation of the pseudo-Hamiltonian and the contribution from 220 more plane waves is added by perturbation theory.[26,27] For the cubic zinc-blende structures the numbers of plane waves used were 27 and 142, respectively. The energy bands obtained from these calculations are shown by the solid lines in Figs. 1 and 2. The calcula-

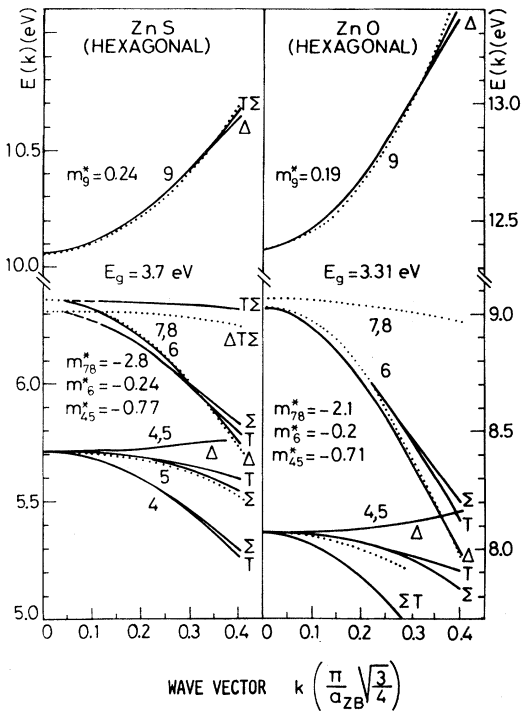

FIG. 1. Energy bands of the wurtzite-type crystals along the Δ, T, and Σ symmetry axes. The calculated bands are represented by solid lines, while the dotted lines indicate the corresponding average spherical (exact parabolic) bands. In cases where the calculated bands and the average spherical bands coincide, only the dotted lines are shown. The m^* given in the figure are the isotropic effective masses which were deduced from the dotted bands. The m^* values cited are in units of the free-electron mass m_0. The a_{ZB} used in the units of the wave vector $\vec{k}$ is the lattice constant of the equivalent zinc-blende structure ($a_{ZB}=\sqrt{2}\,a_{wur}$, where a_{wur} is the lattice constant of the wurzite structure).

tions were carried out in $\vec{k}$ space in a sphere around $\vec{k}=0$ along the main symmetry axes Δ, Λ, and Σ of the cubic ZnS crystal and Δ, T, and Σ of the hexagonal ZnS and ZnO crystals. The radius of this sphere was 0.4 of the distance between the points Γ and A in the hexagonal Brillouin zone, and the intervals between the calculated points were 0.05 of this distance.

In order to justify the approximation of the average spherical band model used in this work, the energy bands along the three different axes are represented one above the other in Figs. 1 and 2. The notations of the appropriate axis and band number are given in the figures near each curve. In the wurzite structure, bands 6–8 are the highest valence bands while band 9 is the lowest conduction band. In the zinc-blende structure, bands 2–4 are the highest valence bands and band 5 is the lowest conduction band. An examination of Figs. 1 and 2 immediately shows that the conduction bands and the light hole valence bands are almost spherical. The heavy hole valence bands in the hexagonal ZnO and ZnS crystals are also almost spherical. The heavy hole band in the cubic ZnS, and the 4 and 5 deeper valence bands in the hexagonal ZnS and ZnO crystals are not spherical and it seems that the approximation of taking an average spherical effective mass for them is somewhat less justified. However, since the joint densities of states of the valence and conduction bands are the significant parameters which enter into the TPPC calculations, and since these joint densities of states for the nonspherical bands depend mainly on the value of the spherical conduction-band effective mass, the average spherical bands model is still a good approximation here.

An examination of the structure of the top of the hexagonal ZnS valence bands in Fig. 1 shows that the band of the light holes near $\vec{k}=0$ is higher than the band of the heavy holes. This wrong behavior is a result of the very rough interpolation scheme used in Ref. 27 to determine the form factors which are used here. In addition, as noted in Ref. 27, no attempt was made to achieve a convergence of the energy bands better than 0.1 eV. However, the correct result for the structure of the top of the valence bands, obtained here for the ZnO crystal, proves that our computation program is essentially correct and that the corresponding wrong structure obtained for the hexagonal ZnS crystal is not due to an error in our calculations. Since no severe problems arose in our calculation because of the wrong valence-band structure of the hexagonal ZnS crystal, the old form factors were used unchanged.

In order to compare the measured and the calculated TPPC results [See Eqs. (7) and (1)], it is necessary to give the values of the mobilities, the lifetimes, and the dielectric constants in the transparent region of the crystals used in the calculations. The values used are $\mu = 200$ cm^2/V sec, $\tau = 10^{-10}$ sec, and $\epsilon = 4$ for the ZnO crystal[5] and $\mu = 100$ cm^2/V sec, $\tau = 10^{-9}$ sec, and $\epsilon = 5.5$ for the ZnS crystal.[31,32] The values of the carrier lifetimes should be considered as order of magnitude values, since they are different for each specific crystal, and depend strongly on the types of the impurities, their concentration, the defects in the crystal, etc. However, in a separate measurement which will be described below, an upper limit to τ was found. We found that our ruby laser, when operated at high pumping intensities, was partially mode locked. As a result, the dye lasers which were pumped by the ruby laser, or by its second harmonic, were also partially mode locked. (Note that in our previous measurements[11–13] the beams of the lasers were not mode locked, since we used low optical pumping intensities for the ruby laser.) This enabled us to check whether the TPPC signals from the ZnS and ZnO crystals followed the pulse shape of the partially mode locked laser beams or not. It is found that the TPPC signals traced the mode locked pulse shape of the laser beams fairly well, and since the round trip in the ruby laser cavity

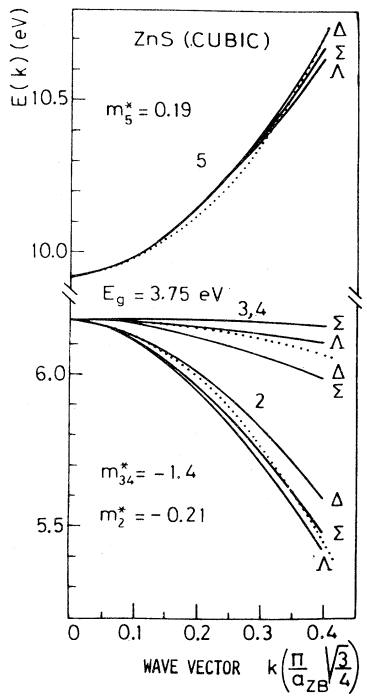

FIG. 2. Energy bands of the zinc-blende ZnS crystal along the Δ, Λ, and Σ symmetry axes. The other notations are the same as those of Fig. 1.

was approximately 4 nsec, one can draw the conclusion that τ for these crystals is less than a few nsec. For a similar measurement in GaAs, where $\tau = 10^{-10}$ sec was measured, see Ref. 8.

The spectral TPPC dependences are shown in Figs. 3 and 4; they were obtained for uniformly scattered and randomly polarized light sources, using Eqs. (1), (7), and (16). These results were calculated within the framework of the simple first approximation which assumes real, constant, and equal MME. The summation over the intermediate bands in Eq. (16) involved all the bands between 4 and 17 in the hexagonal crystals, and between 2 and 10 in the cubic crystal, where the bands notations of Figs. 1 and 2 are used. The values used here for the energies of the fundamental gap $E_g = E_9 - E_7$ and for the second gap $E_9 - E_4$ at $\vec{k} = 0$ were respectively 3.38 and 4.25 eV for the ZnO crystal and 3.82 and 4.57 eV for the mixed ZnS crystal. These values were determined in the spectral TPPC measurements.[12,13] The average effective masses used here are given in Figs. 1 and 2. These values were obtained from the dotted lines in these figures, which represent averages of the energy bands over the different symmetry axes in $\vec{k}$ space.

An obvious limitation of this approximation is the assumption that the MME are real and not complex. Some terms in Eq. (16) however, have negative denominators. Now if we assume that all the allowed MME are real, constant, and equal, then in the summation of Eq. (16) different terms with different signs will cancel each other. But in reality this cancellation strongly depends on the phase of the different complex terms. In order to overcome this difficulty the summation over the intermediate states in Eq. (16) was taken over the absolute values of each term, so that the influence of the phases of the different MME became insignificant. Braunstein and Ockman[15] called this procedure "the incoherent photon approximation." Later on in discussing the results of our third approximation, we will come back to this problem.

Let us for convenience now define a new notation for the transitions in the crystals. Let T_1 denote the transition at the fundamental gap of the crystals, i.e., the transitions from bands 6–8 to the conduction band 9 in the wurzite-type crystals and the transitions from the 2–4 bands to the conduction band 5 in the zinc-blende-type crystals will be called T_1 transitions. The transitions from the 4 and 5 bands to the conduction band 9 in the hexagonal crystals will be called T_2 transitions. The results shown in Fig. 3 for the hexagonal ZnO crystal clearly indicate that the experimentally measured relative magnitude of the T_2 to the T_1 transitions cannot be fitted into the framework of the equal and constant MME approximation. We therefore increased one set of transition MME: $P_{4\to7} = P_{4\to8} = P_{5\to7} = P_{5\to8} = P_1$, where P_1 is a short notation, in comparison with the other MME and a better agreement with the experiment was obtained. In Fig. 4 the theoretical results for the mixed cubic and hexagonal ZnS crystal are described together with the experimental TPPC.[12]

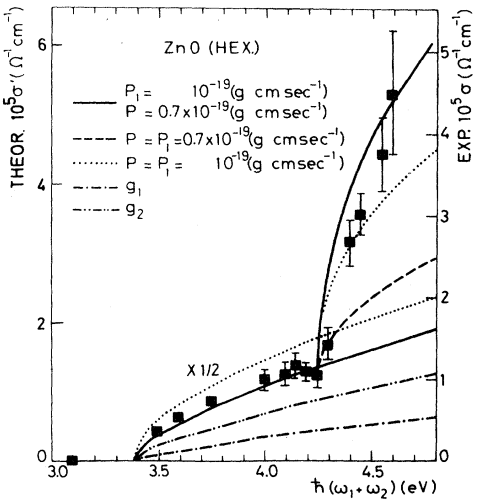

FIG. 3. Theoretical TPPC spectra (σ') in the framework of the real, constant, and equal MME. The experimental results σ (the squares) are those which appear in Fig. 4 in Ref. 13, where the intensities of the beams are $I_1 = 10^{23}$ and $I_2 = 10^{25}$ photons/cm^2 sec and the photon energy of the strong beam is $\hbar\omega_2 = 1.54$ eV. The theoretical calculations were carried out with the same beam intensities and photon energies.

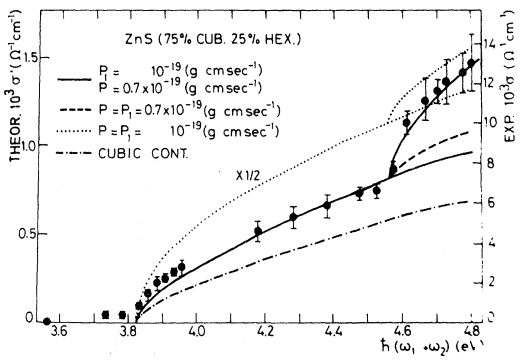

FIG. 4. Theoretical TPPC spectra (σ') in the framework of the real, constant, and equal MME. The experimental results σ (the circles) are those which appear in Fig. 3 of Ref. 12, where the intensities of the beams are $I_1 = 10^{23}$ photons/cm^2 sec and $I_2 = 16$ MW/cm^2, and the photon energy of the strong beam is $\hbar\omega_2 = 1.78$ eV. The theoretical calculations were performed with the same parameters.

The relative quantities cited for the cubic and hexagonal parts of the crystal are those of the crystal used in the experiment. This crystal was examined under a polarization microscope and was found to contain approximately 75% cubic structure and 25% hexagonal structure.[33] Here again, as in the case of the ZnO crystal, we had to increase the P_1 MME with respect to the other MME P, in order to obtain agreement with the experimental results.

The next set of calculations involves the computation of the MME with the aid of the pseudopotential wave functions for the various $\vec{k}$ wave vectors. In these calculations the intermediate states taken into account are bands 4–9 in the hexagonal structure and bands 2–5 in the cubic case. For each i and j of these bands the values of the MME $|P_{ij}(\vec{k})|$ along the main symmetry axes Δ, T, Σ in the hexagonal structure and Δ, Λ, Σ in the cubic structure were calculated. The results for the absolute values of these transition MME are shown in Figs. 5–8, and as in Fig. 1 and 2, the graphs for the different $\vec{k}$ directions are drawn one on top of the other, with the appropriate axis and transition notation given near each curve. Figures 5–7 are seen to be substantially similar. The left sides of these figures show the intraband MME, which were also calculated analytically, and are given by Eq. (A8) of the Appendix. It can be seen that near $\vec{k}=0$ the $|\vec{P}_{ii}(\vec{k})|$ depend linearly on the wave vector $\vec{k}$, and that this behavior continues to approximately 20% of the distance between Γ and A of the hexagonal Brillouin zone. However, this is not always the case. For the ZnO along the T and Σ axes near $\vec{k}=0$ one observes deviations from linearity. Moreover, the MME $P_{6\to9}$ and $P_{7\to9}$ for ZnO along the T and Σ axes show a rapid variation as a function of $\vec{k}$ near $\vec{k}=0$, in contrast to the parallel case of ZnS. The source of this behavior is not clear to us, and calculations of the MME along different axes which are located between the T and Δ axes and between the Σ and Δ axes show that the corresponding values of the MME are found between the limiting values along the T, Σ, and Δ axes and much closer to the values along the Δ axis. Therefore, since this problem occurs only for a few transitions, and mainly in the $T\Sigma$

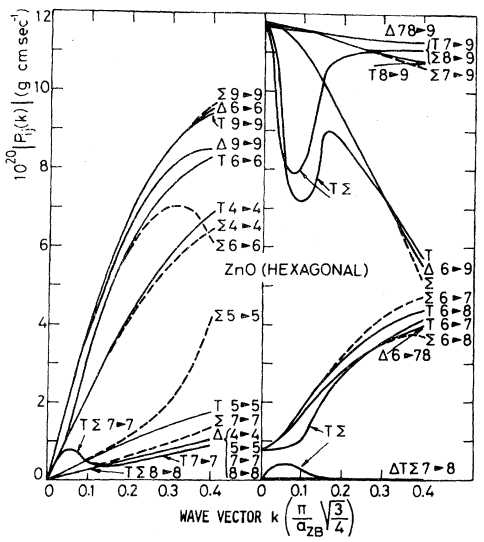

FIG. 5. Absolute values of the intraband and interband transition MME which were calculated in the EPM along the main symmetry axes in the Brillouin zone. The $|\vec{P}_{ij}(\vec{k})|$ MME are indicated in the figure by $Xi\to j$, where X is the axis in $\vec{k}$ space and $i\to j$ represents the transition from the ith band to the jth band.

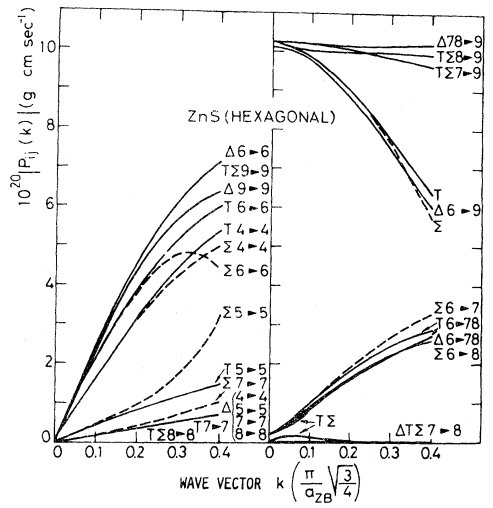

FIG. 6. As in Fig. 5.

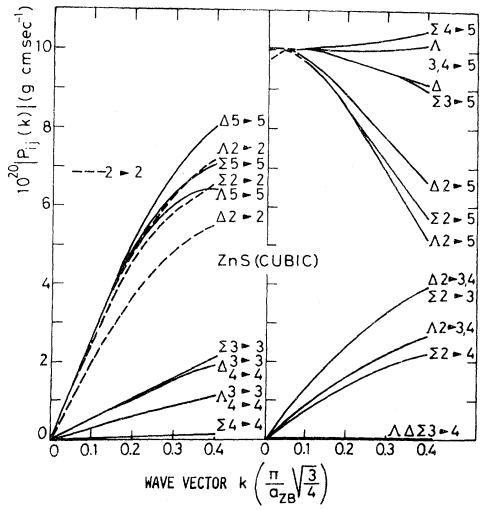

FIG. 7. As in Fig. 5.

plane in $\vec{k}$ space near $\vec{k}=0$ where the joint density of the states is low, an average value of the corresponding MME was used for these rapid variations. Figure 8 shows the MME which are concerned with the transition from the 4 and 5 bands. It is clear that the very complex structure observed cannot be handled by our average isotropic bands approximation. However, a more severe problem arises from the fact that the absolute values of the MME $P_{4,5\to7,8}$ (P_1 in the earlier notation) are smaller by approximately an order of magnitude than the other allowed MME at $\vec{k}=0$ which are shown in Figs. 5–7. We shall discuss these problems in Sec. IV. In order to achieve agreement with the experimental TPPC results, we will assume here that the value of P_1 is approximately ten times higher than its calculated value at $\vec{k}=0$. Figures 9 and 10 show the TPPC results in the present approximation, and the exact values of the P_1 used are given in the captions of these figures. The energies of the fundamental (T_1) gaps used here are those obtained in the pseudopotential calculations, i.e., 3.31 eV for the ZnO crystal and 3.75 eV for the mixed ZnS crystal. For the T_2 energy gap, the experimental values cited above in connection with the first approximation scheme were used. The similar behavior of almost all the MME along the different symmetry axes in $\vec{k}$ space (see Figs. 5–7) allows us to calculate the TPPC within the framework of the spherical bands approximation. The $|\vec{P}_{ij}(\vec{k})|$ for each two bands i and j were averaged over the three different directions in $\vec{k}$ space and the resulting isotropic values were interpolated by a few

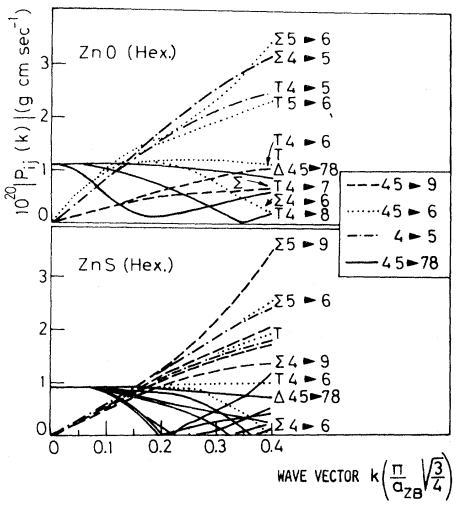

FIG. 8. As in Fig. 5. Because of the complexity of the results for the 4 and 5 bands, only part of the transition MME are shown, and not all of them are specified.

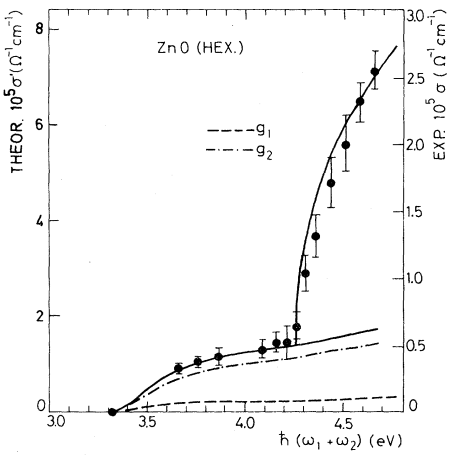

FIG. 9. Theoretical TPPC σ' (the solid line) as it was calculated at the T_1 transition with the aid of the MME which are shown in Fig. 5, and at the T_2 transition with $P_1=10^{-19}$ g cm sec^{-1}. The experimental TPPC (σ) values (circles) are those given in Fig. 3 of Ref. 13, where the beam intensities are $I_1=10^{23}$ and $I_2=10^{25}$ photons/cm^2 sec, and the energy of the photons of the strong beam is $\hbar\omega_2=1.655$ eV.

straight lines in the calculations of the TPPC. This poor interpolation procedure was used here since a more precise calculation will be given later on in our third approximation scheme. In the present set of calculations, as well as in the former set, uniformly scattered and randomly polarized light was considered, and the sum over the intermediate states in Eq. (2) was taken over the absolute values of each of the terms.

The third set of calculations is the most complete and reliable. Two different composite matrix elements were computed. Writing the jth component of the sum in Eq. (2) for uniformly scattered and randomly polarized light, and assuming that the factor of the averages over the

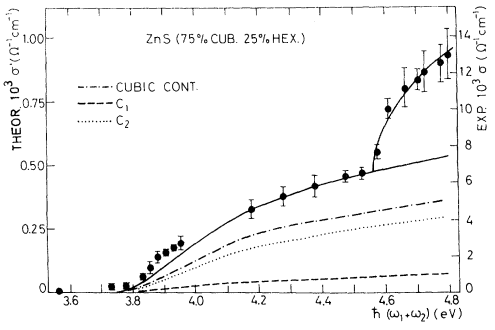

FIG. 10. Theoretical TPPC σ' (the solid line) as it was calculated at the T_1 transition with the aid of the MME which are shown in Figs. 6 and 7, and at the T_2 transition with $P_1=0.9\times10^{-19}$ g cm sec^{-1}. The experimental TPPC σ values are those cited in Fig. 4.

different polarizations of the light sources is one, we obtain

$$M_{vjc}(\vec{k}) = \sum_{l,m=1}^{3} (\vec{P}_{cj}(\vec{k}))_{x_l} (\vec{P}_{jv}(\vec{k}))_{x_m} \times \left(\frac{1}{E_j(\vec{k}) - E_v(\vec{k}) - \hbar\omega_1} + \frac{1}{E_j(\vec{k}) - E_v(\vec{k}) - \hbar\omega_2} \right). \tag{21}$$

The result is that the square of the absolute value of Eq. (2) has the form

$$|M_{cv}(\vec{k})|^2 = \left| \sum_j M_{vjc}(\vec{k}) \right|^2. \tag{22}$$

These squared composite matrix elements were computed for the different valence bands. In addition, the following expressions,

$$[m_{cv}(\vec{k})]^2 = \sum_j |M_{vjc}(\vec{k})|^2, \tag{23}$$

were also calculated for the same valence bands. It is clear that Eq. (23) brings us back to the framework of the former calculations, in the sense that it suppresses the signs of the energy denominators and the phases of the complex transition MME. The results of the computations of both types of composite matrix elements are given in Figs. 11–13. All the computations in this case were done using the exact MME and the exact energy bands which were derived directly from the EPM calculation. In addition, a broadening of the energy denominators of the bands has been included by adding an imaginary width factor of 0.1 eV to the energy denominators of the composite matrix elements. The summations over the intermediate states in Eqs. (22) and (23) were extended over the 67 bands of the hexagonal crystals and over the 27 bands of the cubic crystal. In the process of calculating the summations, printouts of the results were taken at intermediate stages in order to check the convergence in the present and the former approximations. Even with the inclusion of only the highest valence and the lowest conduction bands as intermediate states, the convergence is quite good (up to approximately 80%). For each of the squared composite matrix elements in Eqs. (22) and (23), simple arithmetical averages were taken over the different axes' directions in $\vec{k}$ space. In this averaging procedure the proper weights of the different symmetry axes were taken into account. (The weights taken were 1:1:1 for the hexagonal Δ, T, and Σ axes and 12:8:6 for the cubic Σ, Λ, and Δ axes, respectively.) The resulting isotropic values of the composite matrix elements were interpolated by fifth-degree polynomials with the aid of the least-squares method, and they are shown by the dotted lines in Figs. 11–13. The TPPC was easily obtained by carrying out the analytic integration over $\vec{k}$ space in the isotropic bands approximation, using the same T_1 and T_2 energy gaps as those used

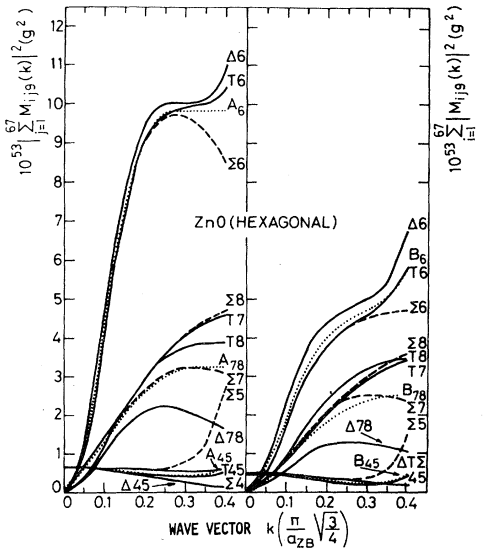

FIG. 11. Composite matrix elements that were calculated in the EPM along the main symmetry axes in $\vec{k}$ space. The notation Xi near each curve indicates that the corresponding composite matrix element belongs to the i valence band along the X axis. The dotted lines indicate spherical averages over the different $\vec{k}$ directions, and are denoted by A_i and B_i for both types of elements. In some unimportant cases a few notations were omitted in the figure because of the lack of drawing space.

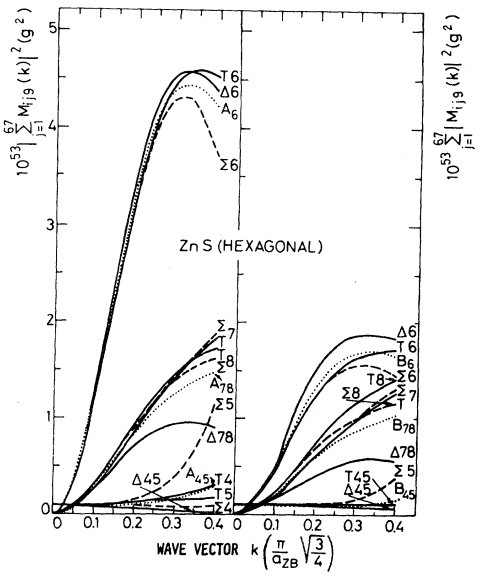

FIG. 12. As in Fig. 11.

in the former approximation scheme. The results of the calculations are shown in Figs. 14 and 15. The results obtained with the composite matrix elements of Eq. (22) are shown by the solid line in these figures and the results using the composite matrix elements of Eq. (23) are shown by the dashed line in both figures. In the second approximation scheme we found that the P_1 is too small in the EPM calculation. For the same reason, the composite matrix elements $|M_{9,4}|^2$, $|M_{9,5}|^2$, $m^2_{9,4}$ and $m^2_{9,5}$ here are also too small. In order to fit the calculations to the experimental measurements, we had to increase each of them by approximately two orders of magnitude. This is equivalent to an order of magnitude increase in P_1. The exact numbers used are given in the captions of Figs. 14 and 15, and the problem itself will be discussed in Sec. IV.

IV. DISCUSSION

Typical results of calculations within the framework of the real, constant, and equal MME are shown in Figs. 3 and 4 for $P = 10^{-19}$ g cm sec^{-1} (the dotted lines) and for $P = 0.7\times10^{-19}$ g cm sec^{-1} (the dashed lines for the T_2 part of the spectra and the solid lines for its T_1 part). Additional calculations show that either an increase or a decrease in the value of these MME only increase the disagreement with the experimental results. It was found that although the relative magnitude of σ' for the T_2 to the T_1 transitions could be fitted with

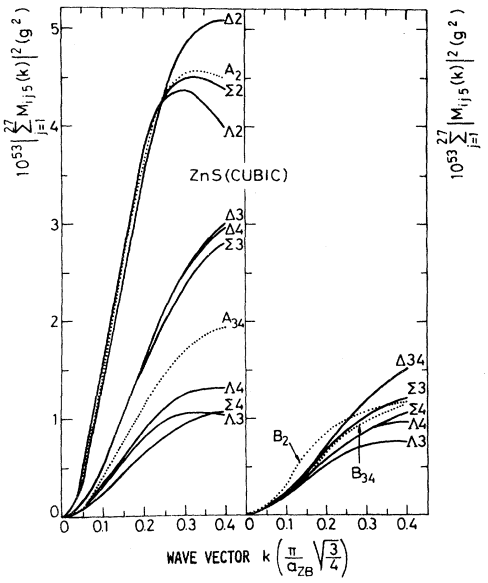

FIG. 13. As in Fig. 11. Graphs of the composite matrix elements $m^2_{5,2}$ were omitted since they overlap those of $m^2_{5,3}$ and $m^2_{5,4}$. However, the average B_2 of $m^2_{5,2}$ is shown in the figure.

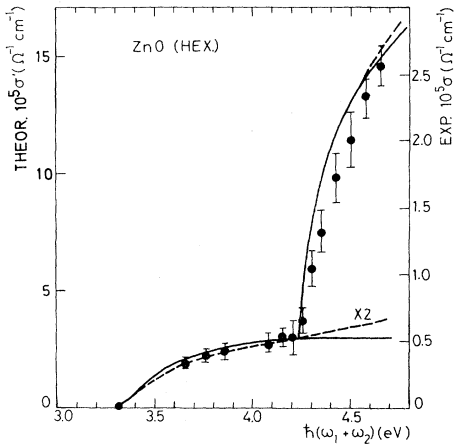

FIG. 14. Theoretical TPPC σ' as it was calculated at the T_1 transition using the composite matrix elements $|M_{cv}|^2$ (the solid lines) and m^2_{cv} (the dashed line) which are shown in Fig. 11. At the T_2 transition $150\times|M_{9,v}(\vec{k}=0)|^2$ and $100\times m^2_{9,v}(\vec{k}=0)$ were used for $v=4,5$, while the composite matrix elements at $\vec{k}=0$ were taken from Fig. 11. The experimental values σ (the circles) are those specified in Fig. 9.

the experimental results, the spectral dependency of the T_1 transition could not. Therefore, in order to increase the relative magnitude of the T_2 transition in comparison with the T_1 transition and keep the correct spectral shape of the T_1 transition, we increased the T_2 transition. This was easily done by means of a small increase in the P_1 MME. As a matter of fact, if we do not want to allow a great change in the specific MME chosen, then P_1 is the only possible candidate for this change. This is because the next-nearest bands connecting bands 4 and 5 through the second-order transition

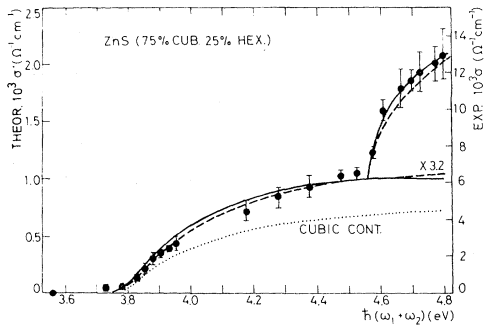

FIG. 15. Theoretical TPPC σ' as it was calculated at the T_1 transition using the composite matrix elements $|M_{cv}|^2$ (the solid line) and m^2_{cv} (the dashed line) which are shown in Figs. 12 and 13. At the T_2 transition we used $450\times|M_{9,v}(\vec{k}=0)|^2$ and $100\times m^2_{9,v}$ for $v=4,5$, while the composite matrix elements at $\vec{k}=0$ were taken from Fig. 12. The experimental TPPC σ (the circles) are those specified in Fig. 4.

probability to the conduction band 9 at $\vec{k}=0$, are bands 11 and 12, which are very far removed from bands 4 and 5 in comparison with bands 7 and 8.[27,29] The energy distance between bands 4 and 5 and bands 11 and 12 is approximately ten times greater than the energy distance between bands 4 and 5 and bands 7 and 8. Should we not want to change P_1 in order to achieve agreement with the experimental results, we have to increase some other MME, for example the set of $P_{4,5\rightarrow 11,12}$, by more than an order of magnitude to achieve this agreement. The value obtained in this way for such MME will therefore be much too high to be of any physical significance, and P_1 was increased instead.

The results of the best fit with the measured TPPC spectra for both kinds of crystals are shown in Figs. 3 and 4 by the solid lines. The shape of the calculated T_1 transition in ZnO is in very good agreement with the experimental results. For clarity, a drawing of the two different contributions to σ' from band 6 and from bands 7 and 8 is also given in Fig. 3. These are indicated by the dash-dot-dash line (g_1) and by the dash-double-dot-dash line (g_2), respectively. The experimental T_2 transition in the ZnO crystal is approximately linear in the two-photon energy, and the theoretical σ' here is an almost exact square root. Hence, no agreement in the shape of the T_2 transition is obtained here and only the magnitude of this transition can be fitted to the experimental results by the adjustment of the P_1 MME explained above. Note that no attempt was made to achieve fine agreement between the calculated σ' and the measured σ because of the great uncertainty in the value of τ used. Hence, although the match of σ' with σ here is remarkable, it should be considered coincidental.

Similar problems appear in the mixed ZnS crystal. The basic change in comparison with the ZnO case was that the total σ' computed was composed of a 75% contribution from the cubic structure and a 25% contribution from the hexagonal structure. The results for σ' in the case where all the MME are equal to $P=0.7\times 10^{-19}$ g cm sec^{-1} (except P_1 which is equal to 10^{-19} g cm sec^{-1}) are shown in Fig. 4 by the solid lines. For this case also shown in this figure is the 75% contribution of the cubic structure to the spectrum, which is denoted in the figure by the dash-dot-dash line. It is interesting to note that the same MME $P_1=10^{-19}$ and $P=0.7\times 10^{-19}$ g cm sec^{-1}, for the two different crystals, yield quite good agreement with the experimental results. This is probably a result of the very close similarity of both ZnS and ZnO crystals. The small deviation of the theoretical σ' curve from the experimental values near the fundamental gap at the T_1 transition may be attributed to the fact that the fractions which were taken for the cubic and hexagonal parts of the mixed ZnS crystal were not exactly determined. Hence, no attempt was made to achieve a better agreement with experiment in this case by a change in the relative magnitude of P and P_1.

An examination of the experimental σ and the theoretical σ' in Fig. 4 shows that the values of σ are greater by approximately an order of magnitude than those of σ'. This discrepancy is much more pronounced than in the parallel case of the ZnO crystal, especially since a good agreement was found there between σ and σ'. Comparing the σ' values of the ZnO and the mixed ZnS crystals at the T_1 transition, one observes that the σ' results for the ZnS crystal are greater by approximately two orders of magnitude than those obtained for the ZnO crystal. This difference is easily understood if one takes into account the different intensities of the light sources, and the different $\mu\tau$ factors used in the calculations. However, a parallel comparison of the experimental σ values shows that the values of σ for the ZnS crystal are larger by approximately three orders of magnitude than those of the ZnO crystal. Two orders of magnitude of this difference have been explained above. (Note that the calculations were carried out with the same intensities of the light sources as those used in the experiment.) But the differences in the values of μ and τ cannot explain the remaining order of magnitude difference, which is also the approximate difference between the σ' and the σ of the ZnS crystal. This is because the values of μ are quite accurate and the values of τ used (10^{-9} sec) cannot be increased significantly, since an upper limit of a few 10^{-9} sec was measured by us as was described above in Sec. III. Hence it seems that the value of σ was overestimated in the measurements.[12] Possible sources of errors in the determination of the experimental σ in Ref. 12 are as follows: (i) An inaccurate value of the thickness of the mixed ZnS crystal used. This could easily yield a factor of 2, since the crystal was a very inhomogeneous mixed platelet. (ii) The electrodes were mounted on one of the large faces of the platelet and 1 mm apart from each other, while the radiation was incident on the other face of the platelet. Hence, the illumination of the areas above the electrodes yields quite a large contribution to the photocurrent and was not taken into account in deducing the TPPC from the photocurrent measured.

The next step will be to discuss the results shown in Figs. 9 and 10. These results were obtained in our second approximation scheme, whereby the MME were evaluated as a function of the wave

vector $\vec{k}$ in a separate EPM calculation. Let us first discuss the results for the ZnO crystal. In Fig. 9 the dashed line (g_1) and the dash-dot-dash line (g_2) show the contributions from band 6 and bands 7 and 8, respectively, to σ' at the T_1 transition. Figure 5 shows that g_2, which gives the dominant contribution to σ' at the T_1 transition, consists mainly of the $7, 8 \rightarrow 9 \rightarrow 9$ transitions. It also shows that three transitions contribute almost equally to g_1. These are the $6 \rightarrow 6 \rightarrow 9$ and $6 \rightarrow 9 \rightarrow 9$ transitions which give a saturated square-root-like contribution, and the $6 \rightarrow 7, 8 \rightarrow 9$ transitions which contribute to g_1 almost linearly. Note that the difference between the contributions of g_1 and g_2 to the calculated σ' is due not only to the different MME, but also to the difference in the joint density of states of the 7, 8, and 9 bands and of the 6 and 9 bands. This difference in the joint density of states can be clearly seen in Fig. 1.

We see that the theoretical σ' at the T_1 transition in ZnO in the present approximation shows a very good agreement with the experimental results (see Fig. 9). However, a severe problem arises in the calculation of σ' at the T_2 transition. As has already been pointed out, the MME which contributes the most to the T_2 transition near $\vec{k}=0$ is P_1. An examination of Fig. 8 shows that near $\vec{k}=0$ this MME is almost constant, while the other MME between the 4 and 5 bands and the other near bands are all zero at $\vec{k}=0$. Hence one may use the constant value of the P_1 near $\vec{k}=0$ to calculate σ' at the T_2 transition near the T_2 energy gap. If one does so, the resulting TPPC turns out to be approximately two orders of magnitude smaller than the experimental results. We have already mentioned that this wrong result may be attributed to a wrong value obtained by the EPM for the MME P_1 and/or to an incorrect joint density of states of the bands 4, 5, and 9. The second possibility is less likely, since it would have to yield similar curvatures for bands 4, 5 and band 9.

Therefore, it seems that the MME involving the deeper valence bands 4 and 5 obtained by the EPM calculations are incorrect. It is well known that in the EPM one obtains pseudo-wave-functions instead of the real wave functions.[28] The real wave function Ψ is represented by a pseudo-wave-function Φ minus a sum of core states φ_c, such that Ψ is orthogonal to these φ_c. This method of representing Ψ has the important advantage that only a small number of basis functions, usually plane waves, is needed in the expansion of Φ in order to describe Ψ correctly. The resulting Φ is taken as equal to Ψ for all practical purposes, outside the region of the core. In the core region, however, Φ is a slowly varying function which does not have the strong atomiclike oscillations that Ψ has. Thus, since the core is usually small, approximately 0.2 of the nearest-neighbor distance, the pseudo-wave-functions Φ should be able to provide relevant information about bonding character, symmetry, and long-range interactions.[34] However, in calculating the MME with the aid of the pseudo-wave-functions, one carries out an integration over the coordinate space which does include the core regions. Therefore, discounting the atomiclike behaviors of the real wave functions in the calculation of the MME in these regions may, in some cases, cause severe errors in the resulting MME. This is apparently the case for the deeper valence bands 4 and 5 here, for which the electrons are much more localized and atomiclike than they are for the higher valence and conduction bands.

It would be interesting to calculate these MME between the 4 and 5 bands and the 7 and 8 bands (P_1) using a different calculation method, say the Korringa-Kohn-Rostoker (KKR) method. In this method one uses a muffin-tin potential and the core functions are rigorously taken into account. Rössler[35] has reported such band structure calculations for hexagonal ZnS and ZnO crystals. Unfortunately, these computations are complicated, and no calculation of the optical constants was performed. But a qualitative investigation of the atomic character of the wurzite-type crystal valence-band structure[35] shows that bands 1 and 2 are probably populated by the S electrons of the anions (see also Ref. 34). The other valence bands are populated by the four $4S^2$ electrons of the Zn atoms and by the eight P electrons of the anions. (There are four atoms per unit cell, two of each type, in the hexagonal crystals.) The top of the valence bands in these crystals is known to have an atomic P-like character, and therefore bands 3, 4, and 5 must contain S electrons. Thus the P_1 must contain the very large contribution of the S to P transitions.

The results shown in Fig. 9 for the T_2 transition were obtained with $P_1 = 10^{-19}$ g cm sec^{-1}. This value is approximately nine times the value of the P_1 calculated with the aid of the EPM at $\vec{k}=0$, which is shown in Fig. 8. Note that $|P_{7,8\rightarrow 9}|$ at $\vec{k}=0$ are approximately 1.17×10^{-19} g cm sec^{-1} (see Fig. 5), which is of the same order of magnitude as the adjustable P_1 used here. Since of all the transitions involving bands 4 and 5, only P_1 was increased significantly, and since all of them, except P_1, are zero at $\vec{k}=0$, (see Fig. 8) only the $4, 5 \rightarrow 7, 8 \rightarrow 9$ transitions were considered in the calculation of σ' at the T_2 transition. Within the limits of the present assumptions about MME involving bands 4 and 5, there is a fair agreement in the shape of the theoretical σ' and the measured σ. The calculated σ' at the T_2 transition has of

course a square-root-like dependence and not the almost linear dependence which was found experimentally.[13,22] A better agreement between σ' and σ would probably be obtained with a better description of P_1 as a function of $\vec{k}$.

The results for σ' in the mixed ZnS crystals, within the framework of the same approximation scheme, are very similar to those achieved in the ZnO crystal. Figure 10 shows these results. As in the former approximation scheme of constant MME, the experimental points are higher than the calculated TPPC at the beginning of the T_1 transition. The causes of this behavior were discussed earlier in connection with the former approximation. However, here it is reasonably clear that the crude linear interpolation used for the MME in the calculation of σ' causes this discrepancy. For clarity, the different contributions of the cubic parts of the crystal are also shown in Fig. 10. The dashed line (C_1) and the dotted line (C_2) show the contributions to the TPPC of band 2 and bands 3 and 4 respectively. The dominant part of C_2 is contributed by the $3,4 \rightarrow 5 \rightarrow 5$ transitions, while C_1 contains almost equal contributions from the three transitions: $2 \rightarrow 2 \rightarrow 5$, $2 \rightarrow 5 \rightarrow 5$, and $2 \rightarrow 3,4 \rightarrow 5$. The σ' calculated at the T_2 transition in this crystal is in very good agreement with the experimental results. Each of the adjustable $|P_{4,5\rightarrow 7,8}|$ was taken here as $P_1 = 0.9 \times 10^{-19}$ g cm sec^{-1}, which is approximately ten times higher than the corresponding value obtained in the EPM calculations (see Fig. 8) and which is almost equal to each of the MME $|P_{7,8\rightarrow 9}|$ (see Fig. 6). The very good agreement achieved here at the T_2 transition and the only fair agreement achieved at T_2 in the ZnO crystal is rather interesting and cannot be explained on the basis of the present treatment of these transitions. It will be left open to future investigations and will not be treated in this work.

We now turn to the third-approximation results (see Figs. 11–15). In essence, the σ' obtained in these calculations for both types of composite matrix elements is very similar to that achieved using the second-approximation scheme. It turns out that the differences in the accuracy of the results due to the summation over all the intermediate contributing bands are not very significant. The importance of the present set of calculations is that it enables us to perform an exact calculation of the composite matrix elements of Eq. (22) using the complex MME and to examine the convergence of the summations over the intermediate states. The results of the two types of composite matrix elements are very instructive. Firstly, one observes a certain similarity between the $|M_{cv}(\vec{k})|^2$ and the $m^2_{cv}(\vec{k})$. Except for the almost constant values for the deeper valence bands 4 and 5 of the hexagonal structure, all the other composite matrix elements between the upper valence bands and the first conduction band begin with an almost parabolic rise near $\vec{k} = 0$ up to approximately $\vec{k} = 0.1$. It is then followed by a certain linear rise range which is quickly saturated to an almost constant value. With the aid of Eq. (1), these behaviors yield TPPC behaviors of the forms $B^{3/2}$, B, and $B^{1/2}$, respectively, where B is equal to $\hbar(\omega_1 + \omega_2) - E_g$. These qualitative results are seen quantitatively in the exact calculations at the T_1 transitions whose results are shown in Figs. 14 and 15. Secondly, for each crystal, the relative magnitudes of the composite matrix elements computed according to Eq. (22) are not the same as those obtained by using Eq. (23). This behavior is very pronounced in the cubic ZnS crystal (see Fig. 13) where the $m^2_{5,v}$ are almost equal for $v = 2$ and $v = 3, 4$ while $|M_{5,2}|^2$ is larger by approximately a factor of 2 in comparison with $|M_{5,3}|^2$ and $|M_{5,4}|^2$. In any case, the complex matrix elements do not cause any severe cancellations in the summation over the intermediate states. As can be seen in Figs. 14 and 15, there is a certain difference in the magnitudes of σ' obtained in the two types of calculations. This is partially due to the differences in the composite matrix elements, but the main source for the difference is the different constant values used for the $|M_{9,5}|^2$, $|M_{9,4}|^2$, $m^2_{9,5}$, and $m^2_{9,4}$ in order to fit the calculated σ' at the T_2 transition to the experimental results. Note that because of the above-mentioned problems concerning the reliability of the P_1 MME obtained by the EPM calculations, it was felt sufficient here to take a constant composite matrix-element value for the $4,5 \rightarrow 9$ transitions.

Another question is the convergence of the summation in Eq. (2) over the intermediate states. It was directly found that for most practical purposes it is enough to take into account only bands 4 to 17 in the hexagonal crystals and bands 2 to 10 in the cubic crystal, as intermediate states. With these intermediate states a convergence of better than 1% was found in the summation of Eq. (2) for both types of crystal, with the sole exception of the problematic 4 and 5 bands. For these latter, the convergence was only accurate up to about 3% for the $|M_{cv}|^2$. However, for the m^2_{cv} the convergence was better than 0.1% for all the bands. The better convergence achieved with the m^2_{cv} in comparison with that achieved with the $|M_{cv}|^2$ is interesting. It is much more pronounced if one takes the summation of Eq. (2) only over the 4–9 bands in the hexagonal structure and over the 2–5 bands in the cubic structure. In this case the convergence of m^2_{cv} is better than (2–3)% and better than 6% for the hexagonal and cubic crystals, respectively.

But $|M_{cv}|^2$ converges only to approximately 20% and (20–30)% for the respective structures. One conclusion from these results is that in the former approximation schemes, where terms of the composite matrix element of type m_{cv}^2 were used, the values achieved for the TPPC were accurate up to approximately (2–6)%. To summarize, for a given degree of accuracy in the calculation of the TPPC, one needs less intermediate bands using m_{cv}^2 than would be necessary if $|M_{cv}|^2$ were used.

Another important question related to all the former calculations is whether occupied states can or cannot be considered as intermediate states in the second-order transition probability $W^{(2)}$. As a matter of fact it was explicitly assumed in this work that occupied states are as good intermediate states as unoccupied ones are. This assumption was used in connection with the T_2 transition. It was assumed that the transitions 4, 5 → 7, 8 → 9 are allowed and contribute to $W^{(2)}$, although the intermediate 7 and 8 bands are occupied by electrons. The question whether an occupied state can be considered as an intermediate state depends on whether the electron which participates in the two-photon transition is actually found in that intermediate state or not. If the electron does not really have to pass through the intermediate occupied state, then this state may be considered virtual. If on the other hand, the electron has to pass through the intermediate state, then the occupied states are forbidden as intermediate states because of the Pauli principle. It is well known and clear that the empty higher bands are good intermediate states. However, no evidence exists that the electrons are really found in these intermediate states. Hence a definite answer to this question is needed before it will be possible to draw conclusions for the occupied states. A solution to these problems is beyond the scope of this article. However, alternative electronic processes may yield results almost equivalent to those obtained if one assumes that occupied states are good intermediate states in $W^{(2)}$. For example, the two-photon transitions 4, 5 → 7, 8 → 9 may be described as a simultaneous double electron jump, in which an electron in the 7 or 8 bands jumps to the conduction band 9 while another electron in band 4 or 5 jumps to the former place of the first electron in band 7 or 8. It is clear that the transition MME for these electronic processes are the same as those found in the parallel case of the two-photon absorption process where the 7 and 8 bands are the occupied intermediate states. Therefore, this double electron jump and the TPA are processes of the same order. Moreover, we have the basic experimental fact that the T_2 transition is stronger than the T_1 transition and as was mentioned above, if one does not want to assume extremely large MME for the 4, 5 → 11, 12 → 9 and/or other transitions, then one is forced to take the 4, 5 → 7, 8 → 9 transitions as the dominant ones at the T_2 transition. There are therefore two possible ways to treat the T_2 transition. The first, which is the most simple and hence assumed here, is that the 4, 5 → 7, 8 → 9 transitions may be handled as regular two-photon transitions, with no attention to whether the intermediate states are occupied or not. The second way, which is only suggested here, is to treat the problem much more carefully, to take into account the problem of occupation of the intermediate states and to consider the different double electron jumps.

V. ALTERNATIVE PROCESSES

Until now it has been basically assumed here that the TPPC process is due to the band-to-band TPA. However, one may also consider alternative processes which yield two-photon photocurrents. Three such processes will be considered briefly in a qualitative way in this section. The first is TPA through defects and impurities, the second is the reabsorption of double or sum-frequency-generated beams in the crystal, and the third is the exciton TPA.

Defects and impurities of a few parts per million or more are usually present in crystals unless special care to avoid them is taken in the growing process. The crystals used in our previous experiments[12,13] contained a fair amount of impurities and defects,[33] and one may ask whether the TPPC measured is not at least partly due to their influence. One definite influence of the impurities on the TPPC can be pointed out immediately. This is the effect of hybrid recombination time which was observed in the measurement of TPPC in ZnS near the crystal gap.[11] The results of this measurement have already been described in Sec. II (see also Fig. 2 in Ref. 12). The influence of such an effect on the TPPC spectra is evident. For example, if the former measurements in the ZnS crystal[12] were performed with a lower intensity of the strong beam, where the linear behavior with smaller slope holds, then the rise of the TPPC as a function of the two-photon sum frequency in the region of the crystal gap would be somewhat smaller than was previously reported. To overcome this difficulty, one can use beam intensities low enough to yield linear TPPC behaviors as a function of one beam intensity while that of the other is kept constant. This, for example, was the case in all our TPPC measurements in the ZnO crystal.[13]

In principle, the impurities may contribute to the TPPC either by the TPA process as initial, intermediate and/or final states, or by cascading double one-photon absorptions. In this latter process, one light beam populates the impurity levels at the crystal band gap, while the other beam transfers the electrons from these levels to the conduction band. In fact, it is quite obvious that any significant contribution to the TPPC by impurities occurs mainly by cascading transitions and not by TPA, since the number of impurities in the crystals is relatively small, and no sharp resonant peaks occur in the TPPC spectra. Hence, only the cascading transition via impurities may be competitive with the band-to-band two-photon electronic transitions. However, the experimental intensity-dependent results[12] imply that the cascadic transitions through impurities do not contribute to the measured TPPC either for the following reasons: (i) Let us first assume that the weak beam populates the impurity levels at the band gap and that the strong beam transfers the excited electrons of these impurities to the conduction band. Such a situation has to yield saturation of the TPPC as a function of the strong-beam intensity, since the strong beam is unable to transfer more electrons to the conduction band than are supplied by absorption of the weak beam. Since no such saturation effect was observed experimentally, this possibility may be dismissed. (ii) Alternatively, let us assume that the strong beam populates the impurity levels at the band gap and that the weak beam transfers the electrons from these levels to the conduction band. In this case the TPPC is expected to be independent of the intensity of the strong beam. The strong beam populates so many electrons at the impurity levels that the weak beam can transfer only a small part of them to the conduction band, i.e., increasing the intensity of the strong beam does not have to yield a similar increase in the TPPC. Since this was not proved to be true experimentally, possibility (ii) must also be discounted. In short, it appears that in our previous measurements[12,13] cascading transitions through impurities did not contribute to the measured TPPC.

Next, we consider the effect of the reabsorption of the sum frequency generated in the crystal and its influence on the measured TPPC. We are mainly interested in comparing the contribution to the TPPC of this sum-frequency reabsorption with the contribution of the band-to-band TPA. For clarity, the simpler case of the second-harmonic generation will be discussed, although the results will be freely used for the sum-frequency generation as well. Several authors have treated the problem of the generated second-harmonic electromagnetic field in crystals. Since the second-harmonic beam is assumed to be totally reabsorbed in the crystal, the simple expression derived by Haueisen and Mahr[36] will be used here. Using somewhat different notations (which will be explained below), Eq. (8) of Ref. 36 yields

$$N_{2\omega} = \frac{(4\pi)^3}{2\hbar\omega c^2} \frac{|d|^2 I_\omega^2}{|\epsilon_{2\omega} - \epsilon_\omega|^2}, \tag{24}$$

where N_ω and $N_{2\omega}$ are the photon densities of the beams of frequency ω and 2ω, respectively, ϵ_ω and $\epsilon_{2\omega}$ are corresponding dielectric constants and $|d|$ is the modulus of the nonlinear susceptibility. In obtaining Eq. (24) the following simple relations of the absolute value I of the Poynting vector were used:

$$I_{\omega_i} = (c/4\pi)\,\epsilon_\omega^{1/2} E_{\omega_i}^2, \tag{25}$$

$$I_{\omega_i} = N_{\omega_i} \hbar\omega_i (c/\epsilon_\omega^{1/2}), \tag{26}$$

where ω_i is either ω or 2ω. Note that the dielectric constant is ϵ_ω in both equations, since the generation rate of the forced second-harmonic wave is due to the fundamental beam,[36] and therefore also Eq. (26) with $\omega_i = 2\omega$ is not the same as the earlier Eq. (4). The photon density in Eq. (24) is due to the nonlinear optical susceptibility and therefore will be denoted by N^{NLOS}. Since the doubled frequency photons are totally reabsorbed in the crystal, N^{NLOS} is also the generated electron density in the conduction band. The electron density obtained in the TPA process, on the other hand, will be denoted by N^{TPA} and is given by $N^{(2)}$ of Eq. (6).

A numerical illustration of a comparison between the N^{NLOS} and the N^{TPA} in the ZnO crystal will now be given. In our experiments[13] the photon flux of the beams ($I_{\omega_i}/\hbar\omega_i$ where $i = 1, 2$) were calibrated to 10^{23} and 10^{25} photons cm^{-2} sec^{-1}. An upper limit value for $|d|$, the nonlinear susceptibility modulus for the ZnO crystal, is approximately 2×10^{-7} esu. This value is achieved by increasing the maximal measured value of $|d(2\omega)| = 2\times10^{-8}$ esu at $\hbar\omega = 1.17$ eV Ref. 37 by an order of magnitude. This procedure seems reasonable since typical variation ranges of the nonlinear susceptibilities when passing from the transparent region to the absorptive region in semiconductors are usually not higher than an order of magnitude.[36,38,39] An examination of the room-temperature dielectric constants of the ZnO crystal[40] shows that no phase matching occurs in Eq. (24), i.e., $\epsilon_{2\omega} - \epsilon_\omega$ does not approach zero for any ω which satisfies $2\hbar\omega > E_g > \hbar\omega$ (where E_g is the crystal energy gap). Hence, using Eq. (24) and assuming $|\epsilon_{2\omega} - \epsilon_\omega| \approx 1$, we obtain the order of magnitude value $N^{\mathrm{NLOS}} \approx 10^4$ electrons/cm^3. In order to find the order of magnitude

of N^{TPA} we will use the expression of $\sigma^{(2)}$ (σ') which appears in Eq. (7). A typical value for σ' in the ZnO crystal is a few 10^{-5} mho/cm (see Figs. 3 and 9). Using also $\mu = 200$ cm^2/V sec and $e = 1.6 \times 10^{-19}$ C in Eq. (7), one obtains $N^{TPA} \approx 10^{12}$ electrons/cm^3. We found that N^{TPA} appears to be larger than N^{NLOS} by approximately eight orders of magnitude. Therefore, in calculating the TPPC and in cases where no phase matching occurs, the reabsorption of the generated second-harmonic or sum-frequency beams is negligible in comparison with the TPA. Moreover, because of the symmetry properties of the nonlinear susceptibility tensor, one can usually choose a special orientation of the crystal for which no sum frequency is generated. An experimental proof that the reabsorption of the second-harmonic-generated light in the crystal does not affect the TPPC was found in Ref. 4 where the TPPC measurements in a hexagonal CdS crystal were found to be independent of the mutual orientations, parallel or perpendicular, of the light polarization and the c axis of the crystal.

Until now, a few examples of processes which may influence the TPA that yield TPPC were discussed. We have seen that these processes, although present, yield only a negligible contribution to the TPPC. There are, however, other possible processes which may affect the TPPC significantly and were not taken into account here. One such process is the exciton TPA. When the crystal is illuminated with light beams whose two-photon energy is close to the absorption edge, the excitons yield most of the TPA. As long as the excitons remain bound electron and hole pairs they are nonconductive, but they may either dissociate into free holes and free electrons or recombine. If they dissociate, which is a reasonable possibility at room temperature, they produce conductive holes and electrons and thereby contribute to the TPPC. This contribution should be wavelength dependent and, in fact, at low-temperature TPA measurements, a series of exciton peaks are usually found.[18,19,21,22] The absence of sharp contributions of excitons at room-temperature TPPC measurements close to the absorption edge of the ZnS and ZnO crystals[12,13] may be due either to the usual weaker exciton influences at room temperature, or to recombination processes which are stronger than the dissociation processes. However, it is possible that the small dip close to the T_2 gap in the ZnO crystal (see the experimental TPPC in Fig. 3 here) is due to the exciton TPA. If this interpretation is correct, it seems that the decrease of TPPC at the exciton levels favors the above-mentioned recombination process over the dissociation process. Only additional TPPC measurements at low temperatures will yield more information about the influences of the excitons on the TPPC spectra.

VI. CONCLUSIONS

The spectral dependencies of the TPPC obtained in the hexagonal ZnO and the mixed cubic and hexagonal ZnS crystals using the various approximation schemes show the following features: (i) The experimental results could be fitted fairly well into all the approximation schemes including the first crude approximation. (ii) At the T_1 transition, substantial agreement with the experimental TPPC results was found in all the different approximation schemes. (iii) At the T_2 transition, only partial agreement with the measurements was found. The relative magnitude of the T_2 to the T_1 transitions was adjusted, but the shape of the spectra agrees well with the experimental results only for the mixed ZnS crystal. In the ZnO crystal (at the T_2 transition), the measurement yields an almost linear rise of the TPPC as a function of the two-photon energies, while the theoretical results show a square-root-like dependence. (iv) In the TPPC results derived with the aid of the composite matrix elements (the third approximation), we find that for uniformly scattered and randomly polarized light sources, the complex character of the MME may influence only the magnitude of the calculated TPPC but not its spectral shape.

Additional general theoretical results obtained in the calculations are as follows: (a) The highest valence bands, although occupied, should be considered as intermediate states in the two-photon transition probability. (b) The pseudo-wave-functions of the deeper valence bands in the hexagonal crystals (bands 4 and 5) are only a poor representation of the real wave functions of these bands. These results were obtained by considering the experimental relative magnitude of the T_2 to the T_1 transitions, and the order of magnitude of the different MME. If one does not allow for MME higher than one or two atomic units, then the dominant contribution to the T_2 transition comes from the occupied intermediate states (bands 7 and 8). Result (b) is obvious since in the pseudopotential calculations only a very small P_1 MME was obtained which cannot explain the measured relative magnitude of the T_2 to the T_1 transitions. Result (a) also suggests that double electron processes may contribute significantly to the TPPC.

It is shown that the experimental procedure used in our previous measurements yields TPPC results which are not affected by TPA by impurities. The influence on the TPPC of the reabsorption

of photons generated by the second-harmonic and/or sum frequencies was found to be insignificant, except for cases where $\vec{k}$ match occurs. The influence of the exciton TPA on the TPPC is considered to be significant in energy regions near the band gaps, but only further experiments at low temperatures will show the exact influence of the excitons.

One important question which was left open to future research is the correct description of the wave functions of bands 4 and 5 in the wurzite-type crystals. This, of course, will also yield the correct $\vec{k}$ dependence of the P_1 MME, which will in turn yield the possibility of calculating the correct spectral shape of the TPPC at the T_2 transition.

ACKNOWLEDGMENTS

The author wishes to express his gratitude to Professor Y. Yacoby for suggesting this problem and for his guidance throughout the work, to Professor W. Low for his interest in this work, for valuable discussions and for revising the manuscript. He further wishes to thank H. Lotem, Professor M. Weger, and Dr. Y. Brada for useful comments and discussions, and Dr. I. B. Goldberg for kindly supplying a special diagonalization computer routine of the complex matrix.

APPENDIX

Using the $\vec{k}\cdot\vec{P}$ perturbation theory we derive a formula for the intraband momentum-matrix element (MME) between the same nondegenerate Bloch's electron states in a crystal, i.e., we are interested in

$$\vec{P}_{ii}(\vec{k}) = \langle \Psi_{i\vec{k}}(\vec{r}) | \vec{P} | \Psi_{i\vec{k}}(\vec{r}) \rangle , \tag{A1}$$

where $\Psi_{i\vec{k}}(\vec{r})$ is the Bloch function of the ith band at the point $\vec{k}$. $\vec{P}_{ii}(\vec{k})$ will be calculated for $\vec{k}$ values near the origin, and for a nondegenerate band i at $\vec{k}=0$, except for time-reversal degeneracy. Substituting the usual form of the Bloch function

$$\Psi_{i\vec{k}}(\vec{r}) = u_{i\vec{k}}(\vec{r}) e^{i\vec{k}\cdot\vec{r}} , \tag{A2}$$

where $u_{i\vec{k}}(\vec{r})$ is its periodic part in Eq. (A1), one easily obtains

$$\vec{P}_{ii}(\vec{k}) = \hbar\vec{k} + \langle u_{i\vec{k}}(\vec{r}) | \vec{P} | u_{i\vec{k}}(\vec{r}) \rangle . \tag{A3}$$

We will now expand the nondegenerate function $u_{i\vec{k}}(\vec{r})$ for $\vec{k}$ values different from zero, in the complete set of functions $u_{i\vec{k}}(\vec{r})$ at $\vec{k}=0$. The coefficients of the expansion are derived from the $\vec{k}\cdot\vec{P}$ interaction Hamiltonian. The result is

$$u_{i\vec{k}}(\vec{r}) = u_{i0}(\vec{r}) + \frac{\hbar}{m} \sum_n{}' \frac{\langle u_{n0} | \vec{k}\cdot\vec{P} | u_{i0} \rangle}{E_{i0} - E_{n0}} u_{n0} , \tag{A4}$$

where E_{n0} are the energy values at $\vec{k}=0$, and the summation is over all the bands n except the band $n=i$. Using Eq. (A4) in order to compute the second term in Eq. (A3) and taking into account only first-order $\vec{k}\cdot\vec{P}$ perturbation terms, we obtain

$$\begin{aligned} \langle u_{i\vec{k}} | \vec{P} | u_{i\vec{k}} \rangle = {} & \langle u_{i0} | \vec{P} | u_{i0} \rangle \\ & + \frac{\hbar}{m} \sum_n{}' \frac{\langle u_{n0} | \vec{k}\cdot\vec{P} | u_{i0} \rangle}{E_{i0} - E_{n0}} \langle u_{i0} | \vec{P} | u_{n0} \rangle \\ & + \frac{\hbar}{m} \sum_n{}' \frac{\langle u_{i0} | \vec{k}\cdot\vec{P} | u_{n0} \rangle}{E_{i0} - E_{n0}} \langle u_{n0} | \vec{P} | u_{i0} \rangle . \end{aligned} \tag{A5}$$

The expression for the effective mass m_i^* of the band i is defined by

$$\left(\frac{m}{m_i^*} \right)_{\mu\nu} = \delta_{\mu\nu} + \frac{2}{m} \sum_j{}' \frac{P_{\mu ij} P_{\nu ji}}{E_i - E_j} . \tag{A6}$$

Hence one can easily see that for a diagonal effective-mass tensor Eq. (A5) may be written in the following way:

$$\langle u_{i\vec{k}} | \vec{P} | u_{i\vec{k}} \rangle = \langle u_{i0} | \vec{P} | u_{i0} \rangle + \hbar\vec{k}[(m/m_i^*) - 1] . \tag{A7}$$

This immediately yields the desired equation for $\vec{P}_{ii}$,

$$\vec{P}_{ii}(\vec{k}) = (m/m_i^*)\hbar\vec{k} + \langle u_{i0} | \vec{P} | u_{i0} \rangle . \tag{A8}$$

It is clear that for centrosymmetric crystals the second term in Eq. (A8) is zero. In addition, a separate independent pseudopotential-band calculation shows that the second term in Eq. (A8) in zinc-blende- and wurzite-type crystals is usually negligible. We will therefore ignore this term. Another interesting result of the pseudopotential-band calculation is that Eq. (A8) may also hold in degenerate cases as well as in nondegenerate cases. This is possible only if the expansion in Eq. (A4) is nondivergent for the given degenerate state. This is so only if the corresponding MME between the degenerate bands in the numerator of Eq. (A4) are all zero. The pseudopotential calculation shows that this is the case for the degenerate valence bands in zinc-blende and wurzite crystals, therefore Eq. (A8) is freely used in the text also for the degenerate valence bands.

[1]J. H. Yee, Phys. Rev. 186, 778 (1969).
[2]F. C. Strome, Jr., Phys. Rev. Lett. 20, 3 (1968).
[3]A. Cingolani, F. Ferrero, A. Minafra, and D. Trigiante, Nuovo Cimento B 4, 217 (1971).
[4]I. M. Catalano, A. Cingolani, and A. Minafra, Phys. Rev. B 5, 1629 (1972).
[5]E. Mollwo and G. Pensl, Z. Phys. 228, 193 (1969).
[6]S. L. Pyshkin, N. A. Ferdman, S. I. Radautsan, V. A. Kovarsky, and E. V. Vitiue, Opto-Electron. 2, 245 (1970).
[7]C. C. Lee and H. Y. Fan, Appl. Phys. Lett. 20, 18 (1972).
[8]S. Jayaraman and C. H. Lee, Appl. Phys. Lett. 20, 392 (1972).
[9]C. H. Lee and S. Jayaraman, Opto-Electron. 6, 115 (1974).
[10]H. J. Fossum and D. B. Chang, Phys. Rev. B 8, 2842 (1973).
[11]G. Koren and Y. Yacoby, Solid State Commun. 11, 239 (1972). Note that in this reference and in Refs. 12 and 13 the units of the conductivities reported should be mho/cm instead of sec^{-1}.
[12]G. Koren and Y. Yacoby, Phys. Rev. Lett. 30, 920 (1973).
[13]G. Koren, Phys. Status Solidi B 61, 277 (1974).
[14]A. Bergman and J. Jortner, Phys. Rev. B 9, 4560 (1974).
[15]R. Braunstein and N. Ockman, Phys. Rev. 134, A499 (1964).
[16]N. G. Basov, A. Z. Grasyuk, I. G. Zubarev, V. A. Katulin, and O. N. Krokhin, Zh. Eksp. Teor. Fiz. 50, 551 (1966) [Sov. Phys.—JETP 23, 366 (1966)].
[17]P. J. Regensburger and E. Panizza, Phys. Rev. Lett. 18, 113 (1967).
[18]D. H. Fröhlich, tenth International Conference on Physics of Semiconductors, edited by xx. Keller (pub. xx, xxx, 1970), p. 95.
[19]F. Fradere and A. Mysyrowicz, Ref. 18, p. 101.
[20]M. S. Brodin, S. G. Shevel, F. F. Kodzhespirov, and L. A. Mozharovskii, Fiz. Tekh. Poluprovodn. 5, 2340 (1971) [Sov. Phys.-Semicond. 5, 2047 (1972)].
[21]W. Kaule, Z. Phys. 256, 97 (1972).
[22]G. Pensl, Solid State Commun. 11, 1277 (1972).
[23]A. Z. Grasyuk, I. G. Zubarev, V. V. Lobko, Yu. A. Matveets, A. B. Mirnov, and O. B. Shatberashvili, Zh. Eksp. Teor. Fiz. Pis'ma Red. 17, 584 (1973) [JETP Lett. 17, 416 (1973)].
[24]M. S. Bespalov, L. A. Kulevskii, V. P. Makarov, M. A. Prokhorov, and A. A. Tikhonov, Zh. Eksp. Teor. Fiz. 55, 144 (1968) [Sov. Phys.—JETP 28, 77 (1969)].
[25]I. M. Catalano, A. Cingolani, and A. Minafra, Phys. Rev. B 9, 707 (1974).
[26]D. Brust, Phys. Rev. 134, A1337 (1964).
[27]T. K. Bergstresser and M. L. Cohen, Phys. Rev. 164, 1069 (1967).
[28]M. L. Cohen and V. Heine, Solid State Phys. 24, 37 (1970), and references therein.
[29]S. Bloom and I. Ortenburger, Phys. Status Solidi B 58, 561 (1973).
[30]J. C. Phillips, Phys. Rev. 104, 1263 (1956).
[31]D. L. Rode, Phys. Rev. B 2, 4036 (1970).
[32]W. Lehman, Bull. Am. Phys. Soc. 3, 45 (1958).
[33]O. Brafman, E. Alexander, B. S. Frankel, Z. H. Kalman, and I. T. Steinberger, J. Appl. Phys. 35, 1855 (1964).
[34]J. D. Joannopoulos and M. L. Cohen, J. Phys. C 6, 1572 (1973).
[35]U. Rössler, Phys. Rev. 184, 733 (1969).
[36]D. C. Haueisen and H. Mahr, Phys. Rev. B 8, 734 (1973).
[37]R. C. Miller, Appl. Phys. Lett. 5, 17 (1964).
[38]M. I. Bell, in *Electronic Density of States*, edited by L. H. Bennett, Natl. Bur. Std. Spec. Publ. No. 323 (U.S. GPO, Washington, D. C., 1971), p. 757.
[39]H. Lotem, G. Koren, and Y. Yacoby, Phys. Rev. B 9, 3532 (1974).
[40]R. Klucker, H. Nelkowski, Y. S. Park, M. Skibowski, and T. S. Wagner, Phys. Status Solidi B 45, 265 (1971).